PAPER

An off-center fed patch antenna with overlapping sub-patch for simultaneous crack and temperature sensing

IOP Publishing Smart Materials and Structures
Smart Mater. Struct. **31** (2022) 095036 (15pp) https://doi.org/10.1088/1361-665X/ac80e0

An off-center fed patch antenna with overlapping sub-patch for simultaneous crack and temperature sensing

Xianzhi Li[1], Songtao Xue[1,2], Liyu Xie[1,*], Guochun Wan[3] and Chunfeng Wan[4]

[1] Department of Disaster Mitigation for Structures, Tongji University, Shanghai, People's Republic of China
[2] Department of Architecture, Tohoku Institute of Technology, Sendai, Japan
[3] Department of Electronic Science and Technology, Tongji University, Shanghai, People's Republic of China
[4] Key Laboratory of Concrete and Pre-stressed Concrete Structure of Ministry of Education, Southeast University, Nanjing, People's Republic of China

E-mail: liyuxie@tongji.edu.cn

Received 14 January 2022, revised 9 June 2022
Accepted for publication 13 July 2022
Published 4 August 2022

Abstract

This paper presents an off-center fed patch antenna for simultaneous crack and temperature sensing. The antenna sensor consists of an off-center fed underlying patch and an overlapping sub-patch. The bottom copper sheet of the sub-patch is tightly attached to the underlying radiation patch allowing the electric current to flow through the integrated patch. The off-center feeding can activate the resonant modes in both transverse and longitudinal directions. The transverse resonant frequencies of the combined patch are utilized for temperature sensing. Therefore, the crack width sensed by the longitudinal frequency shift can be adjusted, eliminating the temperature effect. In addition, this unstressed structure of the combined patch can avoid the issues of incomplete strain transfer ratio and the insufficient bonding strength of a monolithic antenna. The authors developed theoretical relationships between the antenna resonant frequencies, the temperature, and the crack width. They also developed simulations of the off-center fed patch antenna sensor as well as a series of experimental tests to demonstrate the feasibility of the proposed sensor for simultaneous crack and temperature sensing.

Keywords: patch antenna sensor, off-center fed, crack sensing, temperature compensation

(Some figures may appear in colour only in the online journal)

1. Introduction

During the long-term service of civil engineering structures, factors such as structural service loads and environmental effects may cause the degradation of structural performance, posing a danger to the structure's safety and reliability [1]. Therefore, it is necessary to monitor the physical variables revealing the structure's state (e.g. strain, crack, and acceleration) as well as environmental changes, such as temperature and humidity during the service period of a structure, so as to know the structural condition in real time and ensure the safety of the structure [2].

Cracks and structural deformation can explicitly indicate the damage degree of structures. Short-term and long-term effects may widen and extend structural cracks, including differential settlement, excessive loads, material degradation, temperature variation, and so on. The carbonization of concrete and the corrosion of steel bars can accelerate due to the widening cracks, reducing the structure's durability and

* Author to whom any correspondence should be addressed.

bearing capacity. In addition, excessive cracks may lead to a sudden failure or rupture of the structure. Therefore, crack or deformation monitoring should be a critical part of structural health monitoring. Visual inspections and handset measuring with a magnifying lens are time-consuming and frequently inaccurate [3]. With the emerging of artificial intelligence, various image processing technologies have demonstrated great advantages in crack sensing [4–7]. These enhanced vision-based crack detection technologies have the advantage of being non-contact and can lessen the effect of external factors such as the illumination conditions, which can improve crack detection accuracy and efficiency [8]. However, these methods also have drawbacks, such as the requirement to avoid covering the crack's surface and the need for enhanced sensing accuracy [9, 10].

The use of sensors can provide more accurate real-time sensing of cracks. In recent years, some innovative sensors for crack detection have been developed, such as the fiber-optical-based crack sensor [11, 12], the piezoelectric-based crack sensor [13–15], and the crack sensing method based on multi-sensor input and data fusion [16]. On the other hand, sensor-based crack detection technologies usually need cables for power supply and data transmission, resulting in complicated installation and numerous wires. Moreover, some crack sensors focus on crack sensing while disregarding the effects of other factors such as temperature [17], or need additional temperature sensors to measure the temperature for compensation, which also limits their practical use.

In past decades, antenna-based sensing technology has developed rapidly. Antenna-based sensing technology mainly uses the antenna as the sensing unit to measure the desired physical parameters, allowing the antenna to have the dual function of sensing and data transmission. In addition, the antenna's electromagnetic waves can penetrate non-metal coverings, making antenna-based sensing technology better suited for structural health monitoring. Various antenna-based sensors have been proposed for many tasks, including strain sensing [18–20], crack sensing [21], displacement sensing [22–24], temperature sensing [25], humidity sensing [26], bolt loosening detection [27], and cement hydration setting time detection [28]. Some early antenna-based sensors only tracked the change of a single physical variable. For example, the bolt loosening sensor based on patch antenna with overlapping sub-patch only has one resonant mode in the longitudinal direction; thus, the sensor cannot be used for multiple physical variable sensing [27]. The bolt loosening can be accurately detected by the sensor when the external environment remains constant. When the external environment conditions change, such as temperature changes, some errors will occur, and the measurement results need to be corrected. Currently, individual antenna sensors for multiple physical variable monitoring tasks appeared, such as simultaneous strain and crack sensing [29] and simultaneous shear and pressure displacement sensing [30]. Chung *et al* proposed a single-fed patch antenna sensor, in which the change of the fed position can make the patch antenna dual-resonant. The dual-resonant sensor is appropriate for multi-directional strain sensing by a single patch antenna. However, environmental factors such as temperature should be taken into account when using an antenna sensor in engineering tasks [31].

Since temperature fluctuation generates undesirable resonant frequency shifts and inaccurate measurements, temperature effects on an antenna-based sensor should be investigated to improve the sensing performance under variable temperatures [32–36]. Tchafa and Huang developed a strain and temperature sensor based on the microstrip patch antenna, which enabled strain and temperature sensing via two fundamental resonant frequency shifts of a single patch antenna sensor [37]. The strain and temperature alter the antenna sensor's two fundamental resonant frequencies, and the cross-sensitivity between temperature and strain was studied. Tchafa and Huang also proposed a microstrip patch antenna sensor for measuring the dielectric constant of the medium above the antenna as well as the environmental temperature [38]. The preceding studies enabled the antenna sensor to be used when the temperature varies. However, for sensors based on the monolithic patch antenna, the issues of incomplete strain transfer ratio and insufficient bonding strength have limited their use in practice. In this regard, Caizzone and DiGiampaolo proposed a sensor for crack width monitoring based on two mutual coupling planar-inverted F antennas [39]. Xue *et al* proposed an unstressed crack sensor based on a patch antenna fed by capacitive microstrip lines [40], and an unstressed crack sensor based on a patch antenna with an overlapping sub-patch [41]. These unstressed patch antenna sensors can detect crack width variations by the relative movement of the antenna components, avoiding the incomplete deformation transfer ratio and making the measurements more accurate.

To realize the sensing of crack and environmental temperature simultaneously by a single antenna sensor, we propose an off-center fed patch antenna, which can determine the crack width and environment temperature by the dual-resonant antenna, and avoid the problems caused by the monolithic patch. This integrated patch antenna has an off-center fed underlying patch and an overlapping sub-patch. The off-center fed rectangular patch is partially covered by the radiation sub-patch, and the electric current induced by interrogation waves can flow within the combined radiation patch. The off-center fed antenna is dual-resonant; thus, it has two fundamental resonant frequencies, one in a longitudinal direction and the other in a transverse direction. The environmental temperature is the only factor changing the transverse fundamental resonant frequency of the integrated patch since the patch antenna's thermal expansion and the substrate's relative dielectric constant vary with temperature. Nevertheless, the longitudinal resonant frequency of the integrated patch depends on the combined environmental temperature and total electric length as a function of the overlapped length. The overlapped length of the antenna sensor is correlated with the crack width. Therefore, once the temperature is identified by the frequency shift in the transverse direction, the crack width in another direction can realize the temperature compensation. By the decoupling of the two fundamental resonant frequencies in the longitudinal direction and in the transverse direction, the sensor can realize the sensing of multiple physical variables by a single antenna sensor.

This paper is organized as follows. First, the innovative concept of the off-center fed patch antenna with the overlapping sub-patch for simultaneous crack and temperature sensing is introduced. The theoretical relationships between the antenna resonant frequencies, the temperature, and crack width are established. In the simulation study section, the modeling and simulation of the off-center fed patch antenna with overlapping sub-patch are carried out to study the antenna resonant frequencies under different temperatures and different crack widths. In the experimental study section, a series of experimental tests are conducted to show the feasibility of the proposed off-center fed patch antenna sensor for the simultaneous crack and temperature sensing. The last section discusses and concludes the potential and future work of the proposed off-center fed patch antenna sensor.

2. Off-center fed patch antenna with overlapping sub-patch

2.1. Sensing mechanism of the off-center fed patch antenna sensor

The concept and side view of the off-center fed patch antenna with overlapping sub-patch for simultaneous crack and temperature sensing are shown in figures 1 and 2. The patch antenna sensor consists of an underlying radiation patch and an overlapping sub-patch. The bottom copper sheet of the sub-patch is shorted to the underlying radiation patch and can move freely. The effective electric length of the integrated antenna in the longitudinal direction depends on the overall length of the radiation patch and sub-patch. In contrast, the effective electric length in the transverse direction remains the same as that of the underlying patch. An off-center microstrip transmission line feeds the underlying patch antenna with interrogating electromagnetic waves, exciting the integrated antenna's resonant modes both in longitudinal and transverse directions.

According to the cavity model theory, both the patch dimension and relative dielectric constant of the substrate will determine the resonant frequencies of the integrated antenna. The temperature is another vital factor we cannot ignore because it will alter the patch dimension due to the thermal expansion of the antenna. It will also change the dielectric substrate's relative dielectric constant. The resultant effects on the resonant frequency variation of the integrated antenna due to the dimension and the temperature changes will be mixed up. The integrated patch antenna provides a solution to uncouple the effects on resonant frequencies so that we can tracing the dimension and temperature changes simultaneously.

The sensing of the crack width can be achieved by measuring the relative movement between the two components of the antenna sensor. A connecting rod connects the sub-patch to the fixed plate, the underlying patch fastened to one side of the straight crack while the fixed plate is fastened to the other. The copper sheets of the sub-patch and the underlying patch are closely attached as an integrated radiation patch. As long as the crack width changes, the variation causes the relative movement between the two components of the antenna sensor, and the change of the crack width can be sensed by measuring the resonant frequency shift of the antenna. Therefore, there is no limitation on the material what the crack made from. The sensor is suitable for crack sensing of structures made from metal such as steel and aluminum, it is also can be used in some non-metallic objects such as concrete. The overlapped length of the underlying patch and the sub-patch varies as the crack width is increased, causing the antenna resonant frequency shift in the longitudinal direction due to the change in electric length. When the environmental temperature varies, the patch antenna's thermal expansion changes the size of the integrated radiation patch, and the dielectric substrate's relative dielectric constant also fluctuates with the temperature, which results in a shift of resonant frequencies in both the longitudinal and transverse directions. Therefore, the environmental temperature can be determined using the resonant frequency shift in the transverse direction, and the temperature compensation of the longitudinal resonant frequency can be calculated simultaneously. Then, the resonant frequency shift in the longitudinal direction of the patch antenna can be used for the crack sensing. Figure 3 shows the sensing mechanism of the off-center fed patch antenna sensor.

2.2. The off-center fed patch antenna for crack sensing

Figure 1 depicts the off-center fed patch antenna with an overlapping sub-patch. The feeding point is not at the center of the antenna edge; however, the off-center fed can excite the two resonant modes of the antenna. According to the cavity model theory, a patch antenna with an electric length L_e, transverse electric length W_e, and the thickness of the substrate h_e, the resonant frequencies of the patch antenna can be calculated as:

$$f_{mnp} = \frac{c}{2\pi\sqrt{\varepsilon}}\sqrt{\left(\frac{m\pi}{L_e}\right)^2 + \left(\frac{n\pi}{W_e}\right)^2 + \left(\frac{p\pi}{h_e}\right)^2} \quad (1)$$

where m, n and p are the resonant orders in the longitudinal direction, transverse direction, and vertical direction respectively. c is the speed of light in a vacuum; ε is the relative dielectric constant of the dielectric substrate; f_{mnp} represents the resonant frequency when the patch antenna is resonant at the m order in the longitudinal direction, n order in the transverse direction, and p order in the vertical direction. Since the thickness of the substrate is much smaller than the length and width of the patch antenna, the resonant mode of the patch antenna in vertical direction is very weak and can be ignored.

Figure 4 shows the top and side views of the off-center fed patch antenna with overlapping sub-patch. The two copper radiation sheets are closely attached as an integrated radiation patch. The electric length L_e can be calculated as [27]:

$$L_e = L_r + L_s - L_o \quad (2)$$

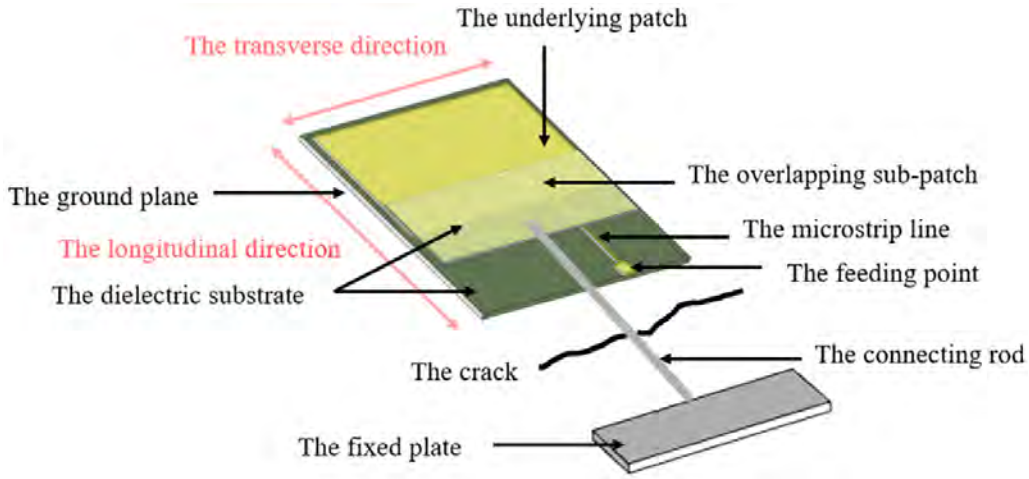

Figure 1. Concept of crack sensor based on off-center fed patch antenna.

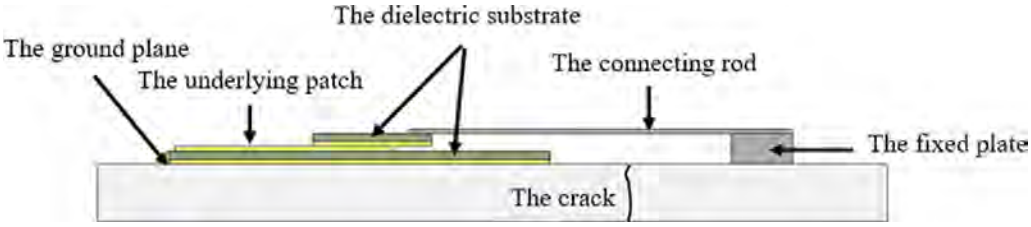

Figure 2. Side view of crack sensor based on off-center fed patch antenna.

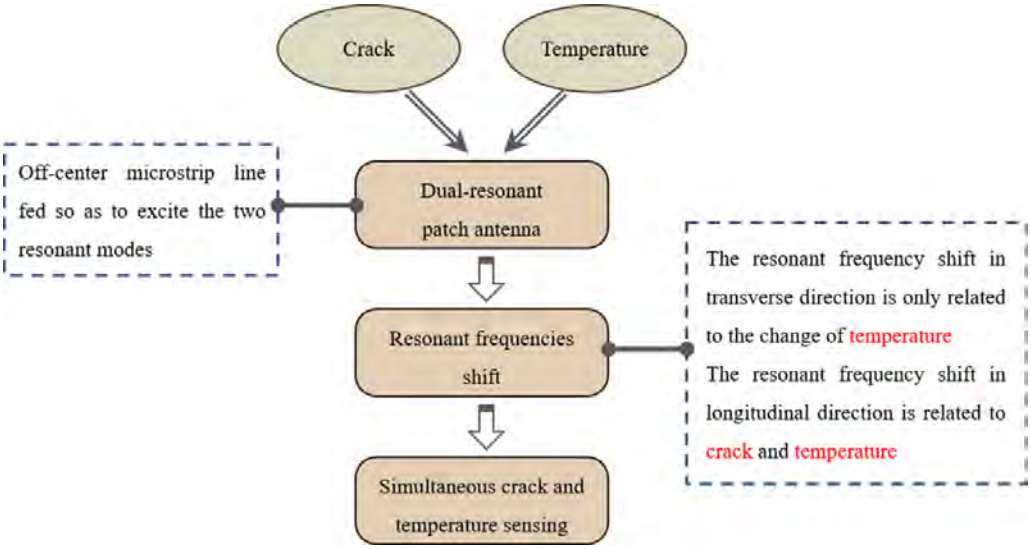

Figure 3. Sensing mechanism of the off-center fed patch antenna sensor.

where L_r is the length of the underlying copper radiation sheet, L_s is the length of the sub-patch copper radiation sheet, and L_o is the overlapped length between the two copper radiation sheets.

When the patch antenna sensor is installed on the surface of the structure and the crack width is extended, the connection between the sub-patch and the fixed plate causes the position of the moveable sub-patch to change, as a result, the overlap length between the underlying patch and the sub-patch changes. The change of the crack width affects the antenna resonant frequency in the longitudinal direction as follows:

$$\begin{aligned} f_{100}(\Delta L_o) &= \frac{c}{2(L_r + L_s - L_o - \Delta L_o)\sqrt{\varepsilon}} \\ &= \frac{c(L_r + L_s - L_o + \Delta L_o)}{2\left[(L_r + L_s - L_o)^2 - (\Delta L_o)^2\right]\sqrt{\varepsilon}} \\ &\approx \frac{c(L_r + L_s - L_o + \Delta L_o)}{2(L_r + L_s - L_o)^2\sqrt{\varepsilon}} \end{aligned} \tag{3}$$

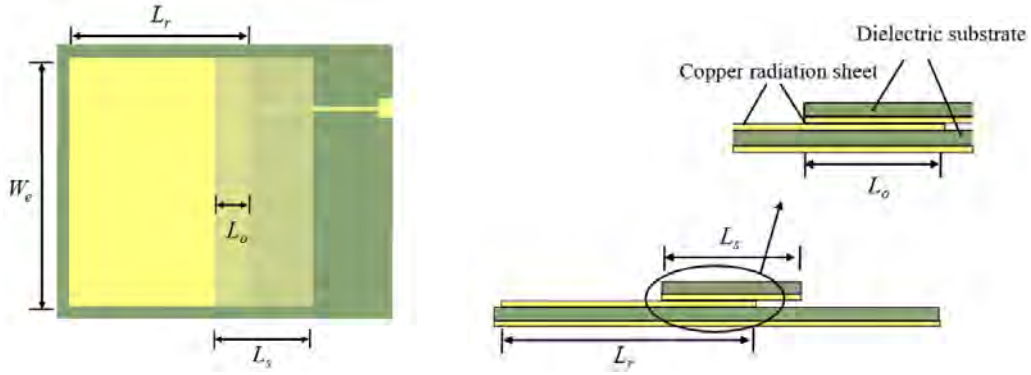

Figure 4. Top view and side view of the patch antenna with overlapping sub-patch.

where ΔL_{o} is the change of the overlapped length and it is equal to the extension of the crack width;

The patch antenna fundamental resonant frequency shift in the longitudinal direction can be calculated as:

$$\Delta f_{100} = \frac{c}{2(L_{\mathrm{r}} + L_{\mathrm{s}} - L_{\mathrm{o}})^2 \sqrt{\varepsilon}} \Delta L_{\mathrm{o}}. \tag{4}$$

The fundamental resonant frequency shift of the patch antenna in the longitudinal direction Δf_{10} changes linearly with the overlapped length ΔL_{o}; therefore, the crack width can be determined by the resonant frequency shift in longitudinal direction.

2.3. The off-center fed patch antenna for temperature sensing and compensation

The temperature variation will affect the patch antenna's integrated radiation patch size and the dielectric substrate's relative dielectric constant, changing the off-center fed patch antenna's two fundamental resonant frequencies. The temperature variation effects can be quantified from two aspects: (a) the patch antenna's thermal expansion and (b) the variations of the dielectric substrate's relative dielectric constant.

Since the underlying patch and the sub-patch are multi-layer laminates, when the environmental temperature changes, internal forces will be generated between layers due to the layers' different thermal expansion coefficients, resulting in a synergistic deformation between layers. When the temperature changes ΔT, the variations in the integrated radiation patch size can be calculated as:

$$\Delta W_T = \frac{\alpha_{\mathrm{d,w}} \Delta T W_{\mathrm{e}} E_{\mathrm{d,w}} h_{\mathrm{d}} + 2\alpha_{\mathrm{c}} \Delta T W_{\mathrm{e}} E_{\mathrm{c}} h_{\mathrm{c}}}{E_{\mathrm{d,w}} h_{\mathrm{d}} + 2E_{\mathrm{c}} h_{\mathrm{c}}} \tag{5}$$

$$\Delta L_T = \frac{\alpha_{\mathrm{d,l}} \Delta T L_r E_{\mathrm{d,l}} h_{\mathrm{d}} + 2\alpha_{\mathrm{cr}} \Delta T L_r E_{\mathrm{c}} h_{\mathrm{c}}}{2\left(E_{\mathrm{d,l}} h_{\mathrm{d}} + 2E_{\mathrm{c}} h_{\mathrm{c}}\right)} + \frac{\alpha_{\mathrm{d,l}} \Delta T L_s E_{\mathrm{d,l}} h_{\mathrm{d}} + \alpha_{\mathrm{c}} \Delta T L_s E_{\mathrm{c}} h_{\mathrm{c}}}{2\left(E_{\mathrm{d,l}} h_{\mathrm{d}} + E_{\mathrm{c}} h_{\mathrm{c}}\right)} \tag{6}$$

where ΔW_T and ΔL_T are the variations of the integrated radiation patch size in the transverse direction and longitudinal direction caused by temperature variations; $\alpha_{\mathrm{d,w}}$ and $\alpha_{\mathrm{d,}l}$ are the thermal expansion coefficients of the dielectric substrate in the transverse direction and the longitudinal direction respectively; $E_{\mathrm{d,l}}$ and $E_{\mathrm{d,w}}$ are the Young's modulus of the dielectric substrate in the longitudinal direction and transverse direction, respectively. h_{d} and h_{c} are the heights of the dielectric substrate and the copper sheet, respectively. α_{c} is the thermal expansion coefficient of the copper sheet, and E_{c} is Young's modulus of the copper sheet.

The relative dielectric constant of the dielectric substrate varies with temperature, which also affects the resonant frequencies of the off-center fed patch antenna. The temperature-dependent relative dielectric constant can be computed as:

$$\Delta \varepsilon_{\mathrm{e}} = k \varepsilon_{\mathrm{e}} \Delta T \tag{7}$$

where $\Delta \varepsilon_{\mathrm{e}}$ is the variation of the dielectric substrate's relative dielectric constant, and k is the thermal coefficient of the relative dielectric constant.

Based on equations (1) and (5)–(7), when temperature changes ΔT, and the overlapped length changes ΔL_{o}, the fundamental resonant frequencies of the patch antenna under the influence of temperature and the overlapped length can be expressed as:

$$\begin{aligned} f_{100}(\Delta T, \Delta L_{\mathrm{o}}) &= \frac{c}{2\left(L_{\mathrm{e}} + \Delta L_T - \Delta L_{\mathrm{o}}\right)\sqrt{\varepsilon_{\mathrm{e}} + \Delta \varepsilon_{\mathrm{e}}}} \\ &\approx f_{100} + \frac{\partial f_{100}}{\partial T} \cdot \Delta T + \frac{\partial f_{100}}{\Delta L_{\mathrm{o}}} \cdot \Delta L_{\mathrm{o}} \end{aligned} \tag{8}$$

$$\begin{aligned} f_{010}(\Delta T, \Delta L_{\mathrm{o}}) &= \frac{c}{2\left(W_{\mathrm{e}} + \Delta W_T\right)\sqrt{\varepsilon_{\mathrm{e}} + \Delta \varepsilon_{\mathrm{e}}}} \\ &\approx f_{010} + \frac{\partial f_{010}}{\partial T} \cdot \Delta T. \end{aligned} \tag{9}$$

Therefore, the environment temperature can be determined by the resonant frequency shift of the off-center fed patch antenna in the transverse direction, and the temperature effects on the resonant frequency of the patch antenna in longitudinal direction can be calculated simultaneously to determine

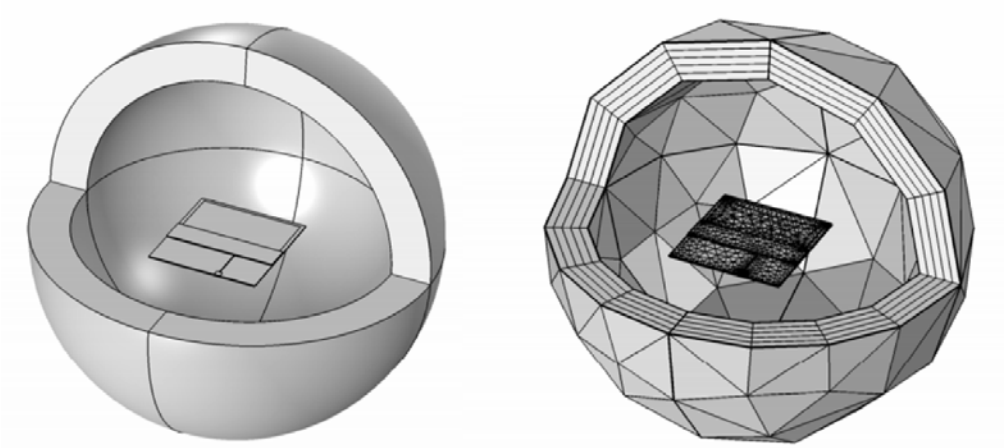

(a) Model of the patch antenna (b) Meshing of the patch antenna

Figure 5. Model of the off-center fed patch antenna with an overlapping sub-patch in COMSOL.

the change of the overlapped length and the extension of the crack width.

3. Simulation study

3.1. The model of the off-center fed patch antenna with overlapping sub-patch

To study the operating performance of the proposed off-center fed patch antenna sensor for the simultaneous crack and temperature sensing, the off-center fed patch antenna with overlapping sub-patch was modeled using COMSOL Multiphysics software. The relationships between the antenna resonant frequencies, the temperature, and the overlapped lengths between the underlying patch and the sub-patch were studied via a series of simulations.

The fundamental resonant frequencies of the patch antenna in transverse and longitudinal direction were designed around 1.95 GHz and 2.6 GHz, respectively. The size of the patch antenna can be preliminarily calculated according to equation (1). Figure 5 shows the modeling of the off-center fed patch antenna with an overlapping sub-patch and the adaptive meshing. The dimensions of the patch antenna are shown in table 1. The material of the radiation sheets was copper, the dielectric substrate of the patch antenna was the Rogers RT/duroid 5880 laminate, and the relative dielectric constant was 2.2. The patch antenna was arranged inside a vacuum sphere with a radius around twice the antenna's maximum size, and the boundary of the vacuum sphere was set as a perfectly matched layer, enabling the electromagnetic wave to propagate into infinite free space. The patch antenna was connected to a lumped port via an off-center microstrip transmission line to excite the antenna and get the patch antenna's reflection loss curve S_{11}, from which the resonant frequencies were calculated.

The basic mechanical and electromagnetic properties of the dielectric substrate material Rogers RT/duroid 5880 and the copper radiation sheet material are shown in table 2.

3.2. The selection of the off-center fed distance

To determine the location of the microstrip transmission line on the off-center fed patch antenna, simulations were conducted to study the relationship between the off-center fed distance and the antenna resonant mode. Figure 6 shows the Smith chart of the patch antenna sensor with different off-center fed distances.

The Smith chart can graphically illustrate the antenna's matching and resonant procedure. When the dots corresponding to the patch antenna's resonant frequencies were near to the center of the circle, it meant that the resonant mode corresponding to that resonant frequency was well excited. The Smith chart shows that when the off-center fed distance was 0 mm, the patch antenna only has one resonant mode in the longitudinal direction, which is around 2.6 GHz. With the distance between the microstrip transmission line and the midpoint of the antenna edge increase, another resonant mode of the antenna in the transverse direction with around 1.95 GHz was gradually excited. The impedance matching of the antenna was satisfactory according to the Smith chart when the off-center feed distance was 8 mm, and the two resonant modes of the patch antenna in transverse and longitudinal directions were well excited. When the off-center fed distance continues to increase, the resonant mode of the antenna in the transverse direction gradually weakens due to the impedance mismatch. Therefore, the distance between the off-center microstrip transmission line and the midpoint of the antenna edge was chosen as 8 mm to excite the antenna's two resonant modes, the longitudinal direction and the transverse direction. Figure 7 shows the reflection loss curve S_{11} of the off-center fed patch antenna with an overlapping sub-patch at 20 °C and a 10 mm overlapped length, the frequencies that correspond to the minimum points of the curve are the resonant frequencies of the patch antenna in longitudinal direction and transverse direction.

Figure 8 shows the antenna's induced current in two fundamental resonant modes. The induced current of the radiation patch and the sub-patch flows along the longitudinal direction

Table 1. The dimensions of the off-center fed patch antenna with overlapping sub-patch.

Parameters	W_e (mm)	L_r (mm)	L_s (mm)	L_o (mm)	h_d (mm)	h_c (mm)
Dimensions	51	36	13	8.0–12.0	0.51	0.07

Table 2. The mechanical and electromagnetic parameters of the antenna material.

Parameters	$\alpha_{d,w}$	$\alpha_{d,l}$	α_c	ε
Value	48 ppm $°C^{-1}$	31 ppm $°C^{-1}$	17 ppm $°C^{-1}$	2.2
Parameters	$E_{d,w}$	$E_{d,l}$	E_c	k
Value	1.07×10^3 MPa	0.86×10^3 MPa	1.1×10^5 MPa	-125 ppm $°C^{-1}$

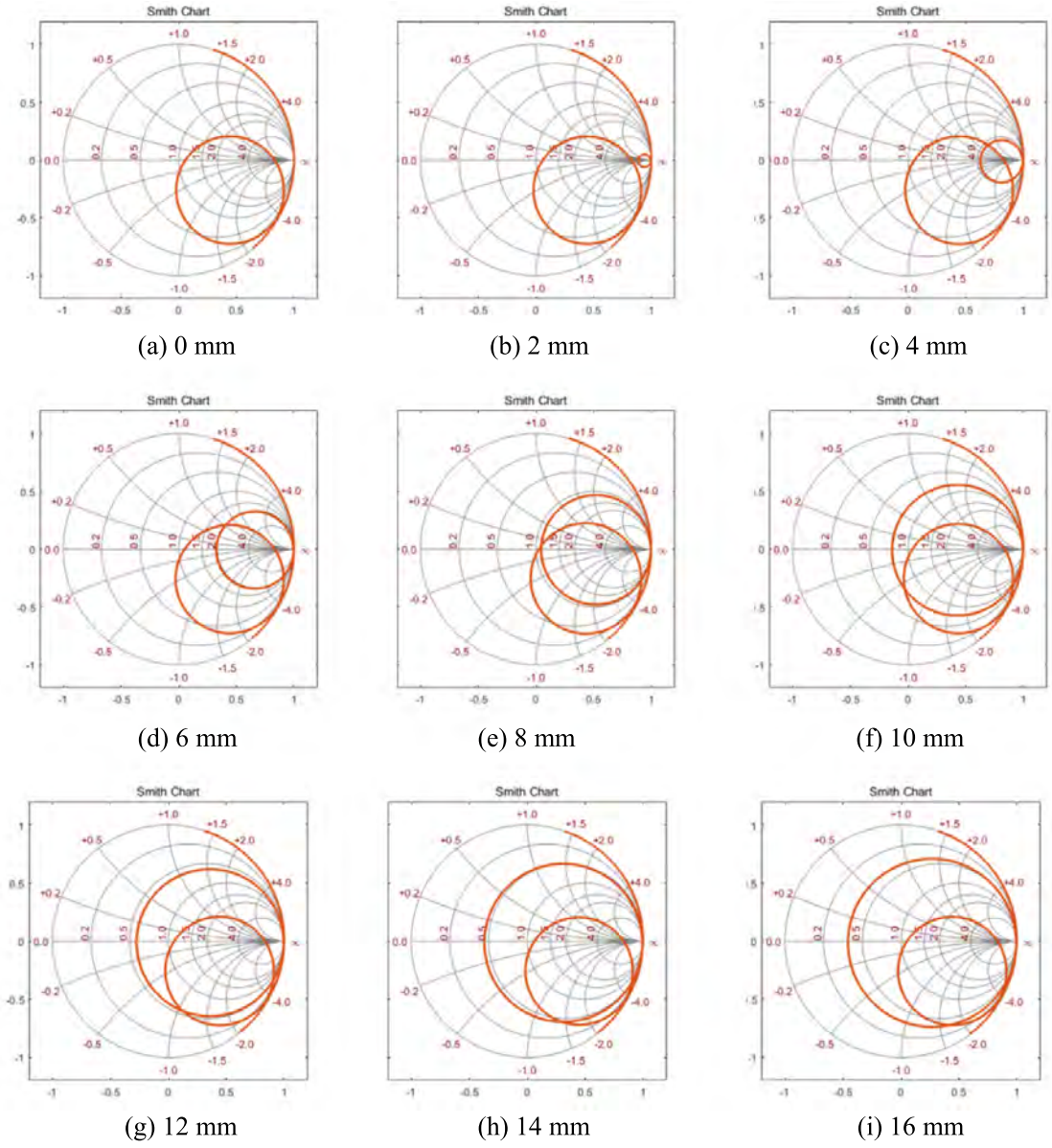

(a) 0 mm (b) 2 mm (c) 4 mm

(d) 6 mm (e) 8 mm (f) 10 mm

(g) 12 mm (h) 14 mm (i) 16 mm

Figure 6. The Smith chart of the patch antenna under different off-center fed distances.

when the antenna resonant at longitudinal direction, while the induced current flows transversely when the antenna resonant at transverse direction. Clearly, the fundamental resonant modes of the antenna were well excited in both the longitudinal and transverse directions. The patch antennas' higher order resonant frequencies in the longitudinal and

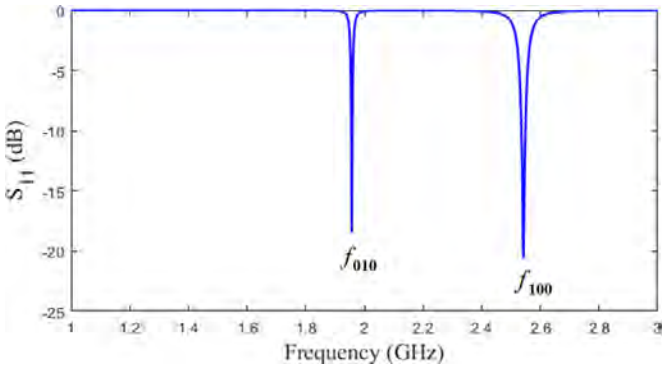

Figure 7. The reflection loss curve of the off-center fed patch antenna with overlapping sub-patch (20 °C, 10 mm overlapped length).

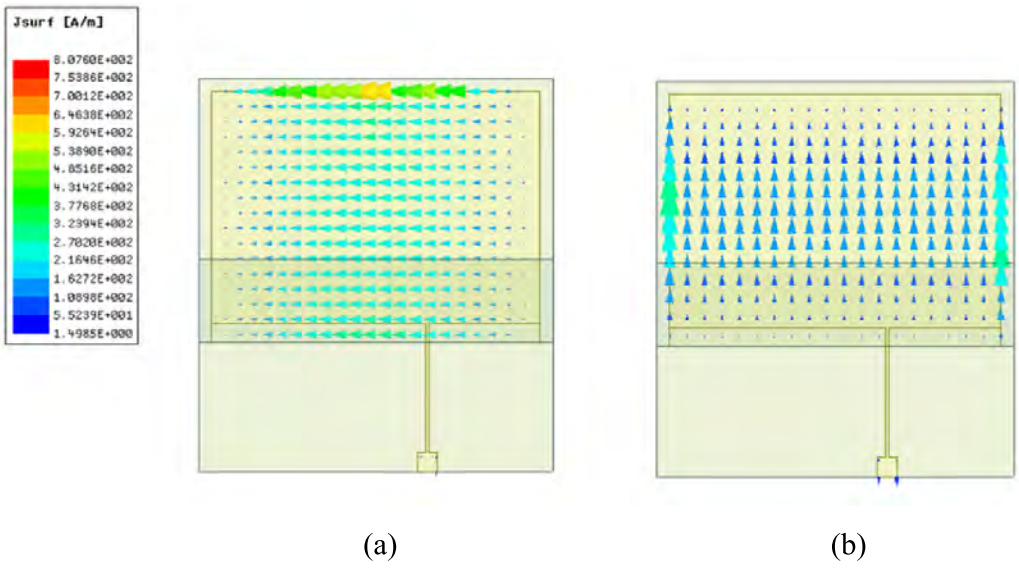

Figure 8. The induced current of the antenna at two fundamental resonant modes is shown in (a) the transverse direction resonant mode and (b) the longitudinal direction resonant mode.

transverse directions are greater than 3 GHz, which are not suitable for measurement by the 0–3 GHz vector network analyzer (VNA) in practice. Therefore, the higher order resonant frequencies of the patch antenna are not discussed in this study.

3.3. The simulation of the off-center fed patch antenna for crack sensing

To study the relationship between the off-center fed patch antenna resonant frequencies and the crack width, a series of simulations were carried out on the off-center fed patch antenna with different overlapped lengths. In the simulation study, the overlapped length changed from 12.0 mm to 8.0 mm to simulate a crack width extension from 0 to 4 mm. The patch antenna was fed by a lumped port via the off-center microstrip transmission line, the sweep frequency range was set to operate from 1 GHz to 3 GHz, and the interval was set as 0.0005 GHz.

Figure 9 shows the S_{11} curves of the off-center fed patch antenna with different overlapped lengths. The frequencies that correspond to the minimum points of the curves are the resonant frequencies of the patch antenna. The simulation results show that when the overlapped length between the underlying patch and the sub-patch varies, the fundamental resonant frequency in the longitudinal direction changes correspondingly while the fundamental resonant frequency in the transverse direction remains constant. The simulation results in figure 10 show that the patch antenna fundamental resonant frequency in the longitudinal direction shifted linearly with the overlapped length. When the overlapped length of the patch antenna changed by 0.1 mm, the patch antenna resonant frequency in the longitudinal direction shifted by about 6.05 MHz; thus, the change in the overlapped length of the patch antenna can be measured accurately by the patch antenna resonant frequency shift in the longitudinal direction, which means the extension of the crack width can then be obtained.

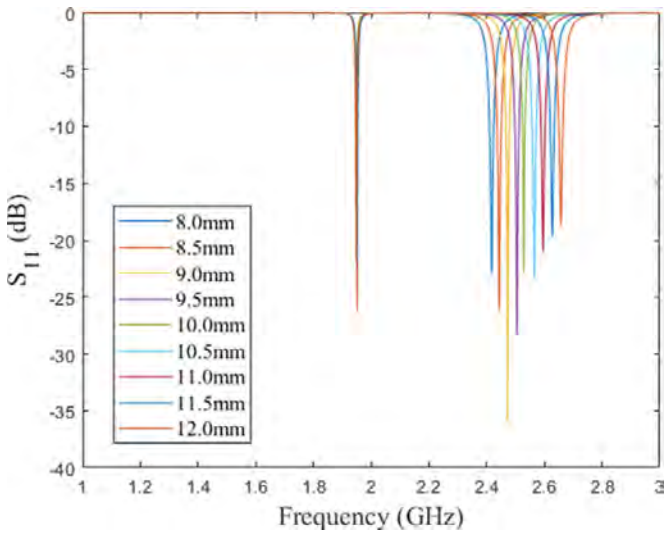

Figure 9. The S_{11} curves of the off-center fed patch antenna with different overlapped lengths.

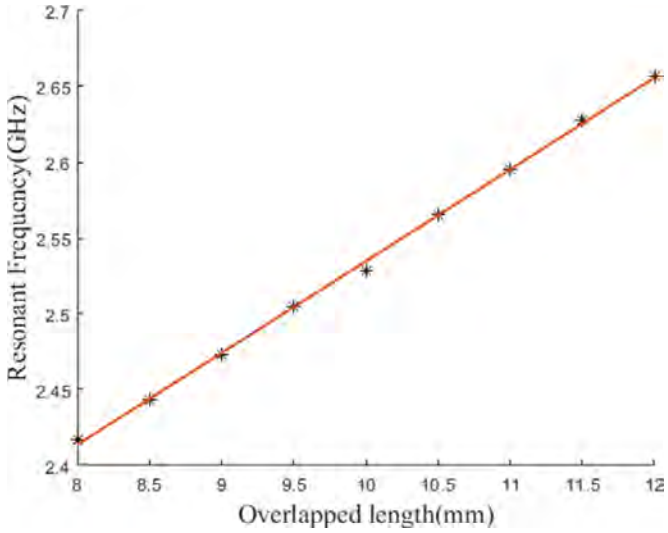

Figure 10. Resonant frequency in longitudinal direction with different overlapped lengths.

3.4. The simulation of the off-center fed patch antenna for temperature sensing

The COMSOL Multiphysics software is suitable for multiple physical field simulations. Since the patch antenna experiences the thermal deformation effect and the relative dielectric constant of the dielectric substrate varies with temperature, the solid mechanics module was used to solve the thermal deformation of the patch antenna first; then, the electromagnetic simulation module was used to get the reflection loss curve S_{11} of the off-center fed patch antenna under different temperatures. In the simulations, the patch antenna was fed by the lumped port via the off-center microstrip transmission line, and the settings of the sweep frequency were set as 1 GHz–3 GHz with a 0.0005 GHz interval. The temperature varies from 0 °C to 50 °C and the simulation results are shown in figures 11 and 12.

The S_{11} curves were utilized to obtain the resonant frequencies of the off-center fed patch antenna at the local minimum points of the curves. The simulation results show that the off-center fed patch antenna resonant frequencies in the transverse direction and longitudinal direction were both affected by the temperature, and the resonant frequencies of the patch antenna shifted linearly with changes in temperature. When the temperature changed 1 °C, the patch antenna fundamental resonant frequency in the transverse direction shifted about 0.134 MHz and the fundamental resonant frequency in the longitudinal direction shifted about 0.169 MHz. The corresponding temperature sensitivity for the fundamental resonant frequency in the transverse direction and the fundamental resonant frequency in the longitudinal direction were calculated theoretically as 0.089 MHz $°C^{-1}$ and 0.134 MHz $°C^{-1}$, respectively. Thus, temperature sensing can be realized by the patch antenna fundamental resonant frequency shift in the transverse direction and the resonant frequency shift in the longitudinal direction under various temperatures can be calculated for the simultaneous crack and temperature sensing.

4. Experimental study

Based on the theoretical research and simulation study, a series of experiments were set up to illustrate the feasibility of the proposed off-center fed patch antenna sensor for simultaneous crack and temperature sensing. The underlying patch and the overlapping sub-patch were fabricated by the chemical etching [42], and the process shown as follows. First, the Rogers RT/duroid 5880 copper clad laminate was cut to the desired size. Then, the thermal transfer printer and the toner were used to print the designed patch shape to the laminate. The laminate coated with toner was placed into the corrosive liquid to etch the unwanted copper, shown in figure 13. After finish the etching, the toner covering the patch should be wash off, the underlying patch and the sub-patch were fabricated shown in figure 14. Finally, the subminiature A (SMA) connector was soldered to the microstrip transmission line in the underlying patch. The off-center fed patch antenna with overlapping sub-patch shown in figure 15. The dimensions of the antenna sensor are shown in the simulation study section.

The patch antenna was fed by a microstrip transmission line, and the distance between the off-center microstrip transmission line and the midpoint of the antenna edge was 8 mm. The off-center microstrip transmission line was connected to the VNA through the coaxial line as shown in figure 16. The VNA was able to analyze the antenna's reflected signal and get the reflection loss curve S_{11} of the off-center fed patch antenna sensor. Then, the S_{11} curves were fitted by the quadratic function in the region surrounding the local minimum point, and the quadratic function curves were utilized to extract the resonant frequencies of the patch antenna sensor. The VNA used in the experiment was a Keysight N5227A network analyzer, the sweeping range of the VNA was set as 1 GHz–3 GHz, and the sweep points were set as 4001 points.

Figure 17 shows the crack extension simulator, which is able to simulate the crack width increase and decrease. The

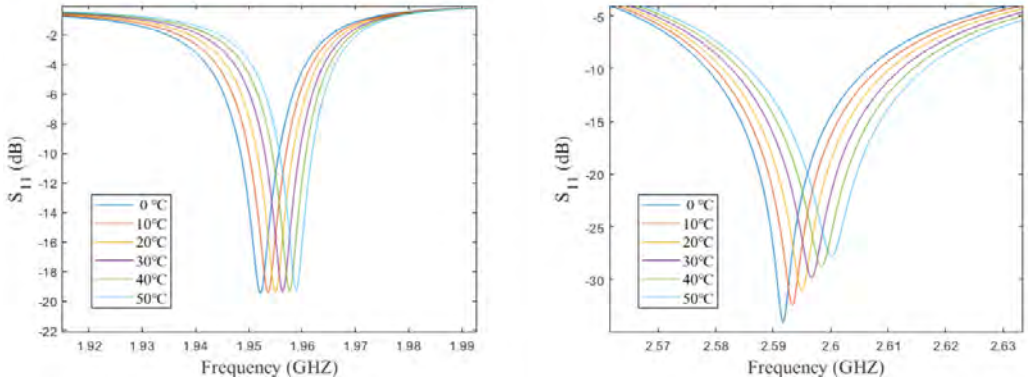

Figure 11. The S_{11} curves of the off-center fed patch antenna under different temperatures in (a) the resonant mode in the transverse direction and (b) the resonant mode in the longitudinal direction.

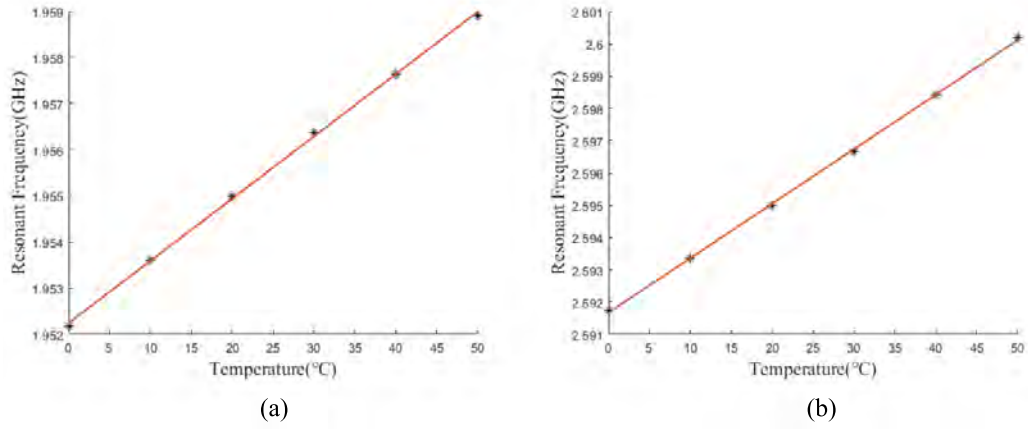

Figure 12. The fundamental resonant frequencies under different temperatures for (a) the resonant frequencies in the transverse direction and (b) the resonant frequencies in the longitudinal direction.

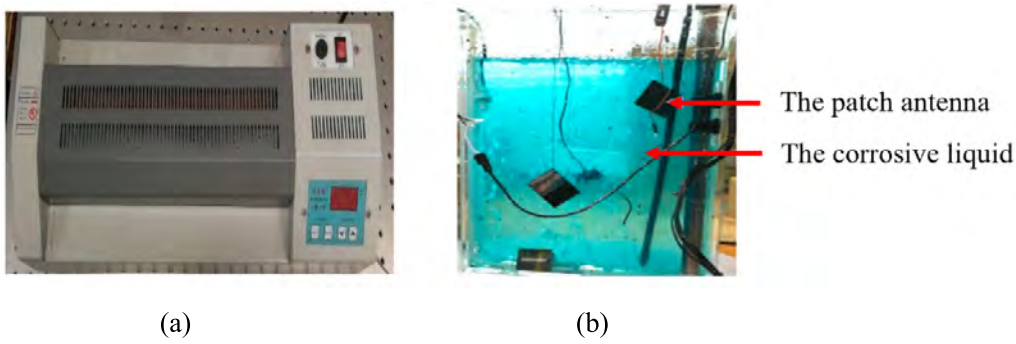

Figure 13. The equipment used in the fabrication process (a) the thermal transfer printer used to print the designed patch shape (b) the corrosive liquid used to etch the unwanted copper.

device has been used in some relevant research to simulate the variation of crack width [40, 43]. The crack extension simulator is comprised of a base plate, a fixed table mounted on the base plate, a moveable fine-tuning table, and a screw micrometer rod. The moveable table could be pushed by the screw micrometer rod and moved relative to the fixed table to simulate the crack width extension. The minimum increment of the screw micrometer rod was 0.01 mm; thus, the crack width variation can be simulated with a minimum precision of 0.01 mm. The off-center fed patch antenna sensor was installed on the crack extension simulator, and the underlying patch was fixed to the fixed table of the crack extension simulator by the glue and fixture. Meanwhile, the sub-patch was glued and fixed to the moveable fine-tuning table by the connecting rod. Figure 18 depicts the experimental setup.

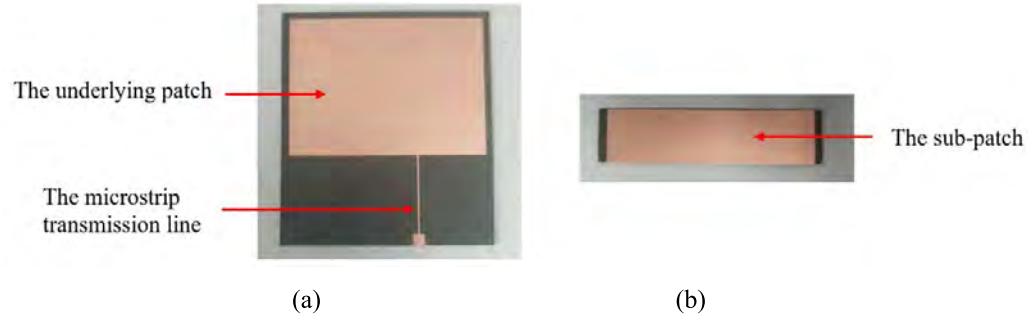

Figure 14. The fabricated antenna (a) the underlying patch (b) the sub-patch.

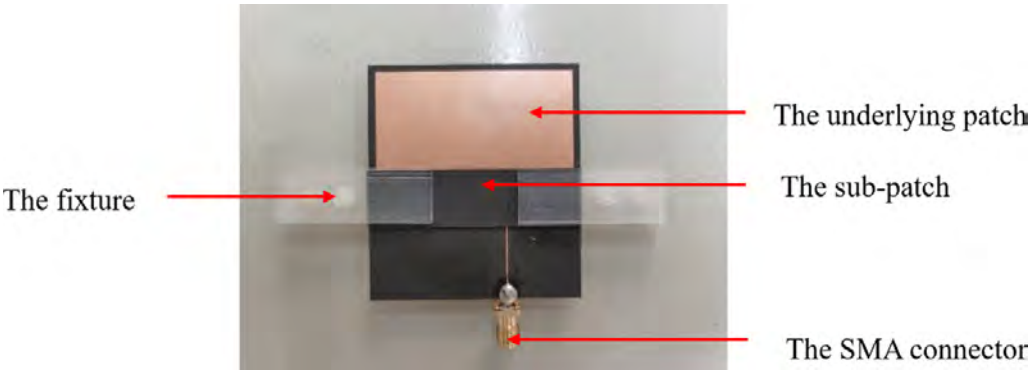

Figure 15. The off-center fed patch antenna with overlapping sub-patch.

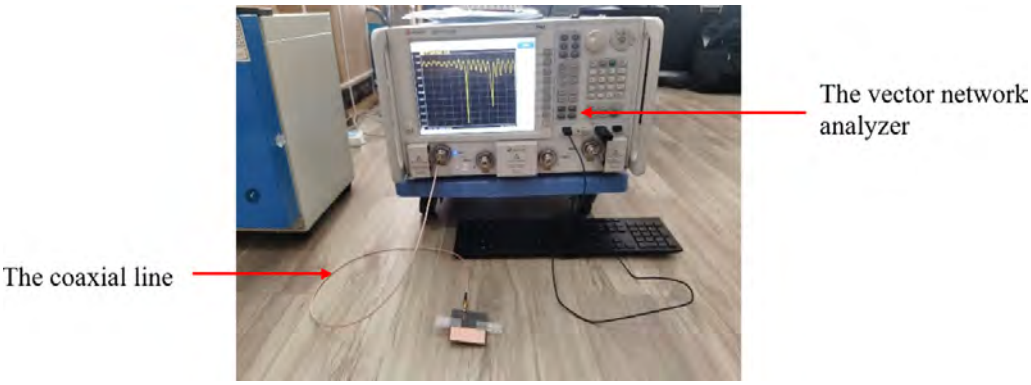

Figure 16. The off-center fed patch antenna connected to the vector network analyzer (VNA).

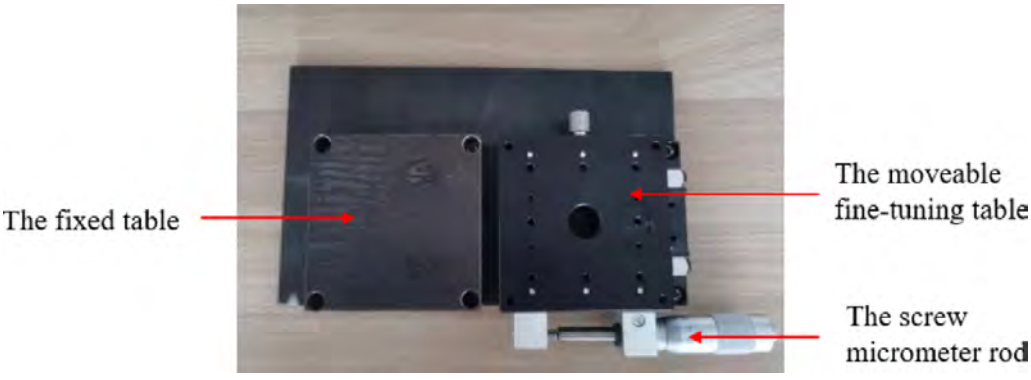

Figure 17. The crack extension simulator.

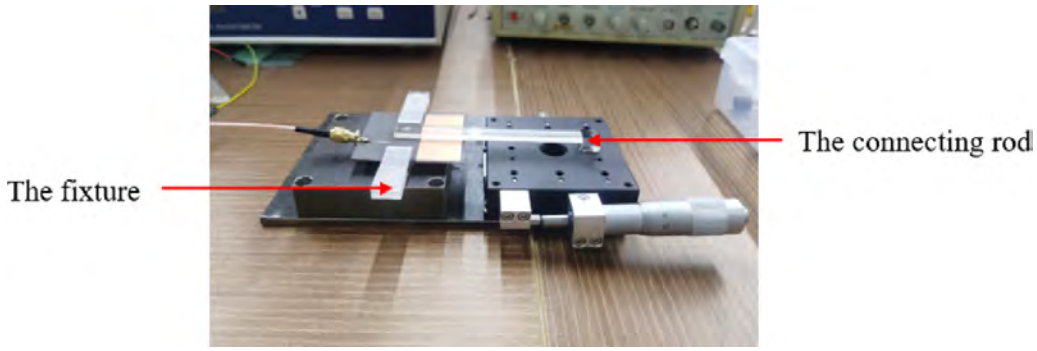

Figure 18. The off-center fed patch antenna and the experimental setup.

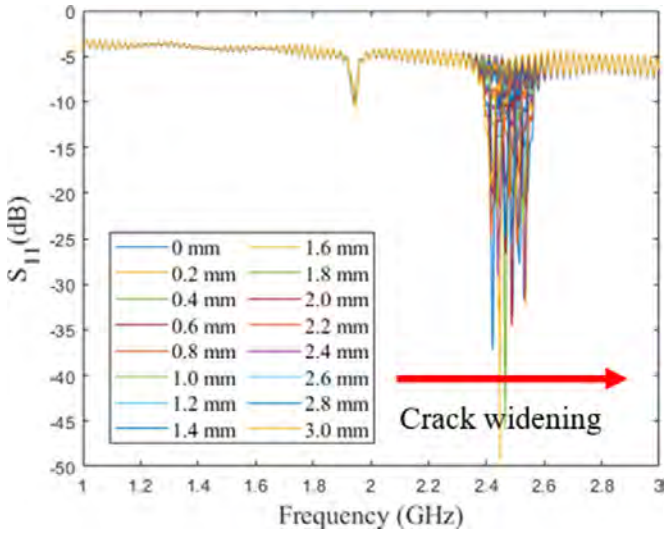

Figure 19. The S_{11} curves of the off-center fed patch antenna with different crack widths.

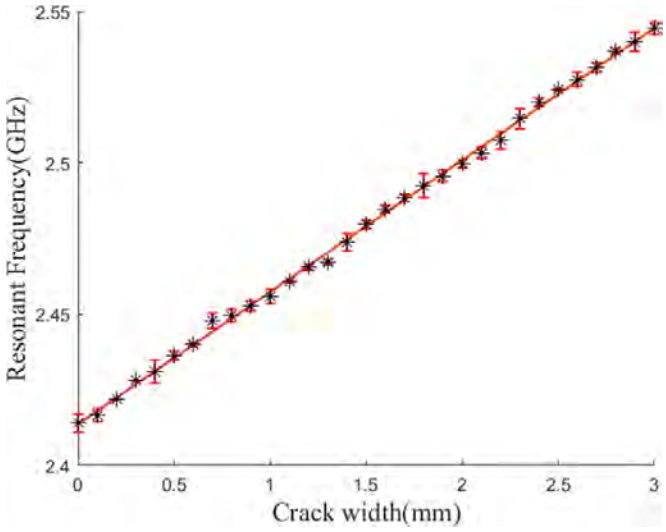

Figure 20. The resonant frequency in the longitudinal direction with different crack widths.

In the crack sensing experimental study, the movable fine-tuning table can move toward and against the fixed table, which was controlled by the screw micrometer rod. When the fine-tuning table moved toward the fixed table, the crack width between the two tables was reduced. Conversely, the crack width between the two tables was increased when the fine-tuning table moved against the fixed table. The simulator simulates crack width extension from 0 mm to 3 mm with a 0.1 mm incremental step. Figure 19 shows the reflection loss curves S_{11} of the off-center fed patch antenna, and figure 20 shows the patch antenna's resonant frequency in the longitudinal direction with different crack widths. To demonstrate the linear trend of the patch antenna's resonant frequency is repeatable, the experimental tests were conducted 5 times, and the standard deviation error bars can be seen in figure 20.

Because the crack width variation changes the relative position of the sub-patch and the underlying patch, the resonant frequency of the off-center fed patch antenna in the longitudinal direction shifts with the crack width extension. The experiment results show that the resonant frequency of the off-center fed patch antenna in the longitudinal direction shifts linearly when the crack width changes, the sensitivity is 43.9 MHz mm^{-1} and the linear trend is reproducible in repeated measurements. Thus, the off-center fed patch antenna sensor can be used to precisely assess the change of the crack width.

To demonstrate the feasibility of the proposed off-center fed patch antenna sensor for temperature sensing, the off-center fed patch antenna was placed in the temperature control box as shown in figure 21. The temperature control box temperatures change from 20 °C to 70 °C with an increment of 2 °C. When the temperature varies, the antenna's integrated patch size and the dielectric substrate's relative dielectric constant changes accordingly. Figure 22 depicts the off-center fed patch antenna's reflection loss curves S_{11} at various temperatures, while figures 23 and 24 depict the patch antenna's resonant frequencies at various temperatures. The experimental tests that the patch antenna sensor under varying temperature scenario were also conducted five times, the standard deviation error bars of the resonant frequency in transverse direction and longitudinal direction can be seen in figures 23 and 24 respectively.

The patch antenna's experimental results under different temperatures show a patch antenna sensor temperature

Figure 21. The off-center fed patch antenna placed in the temperature control box.

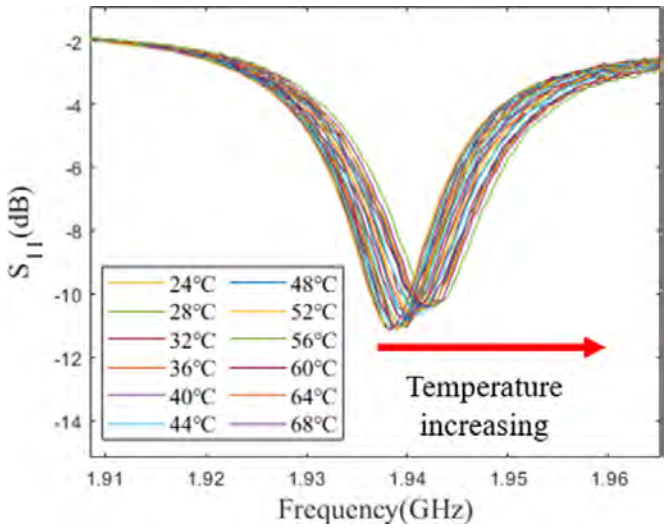

Figure 22. The S_{11} curves around transverse resonant frequency under different temperatures.

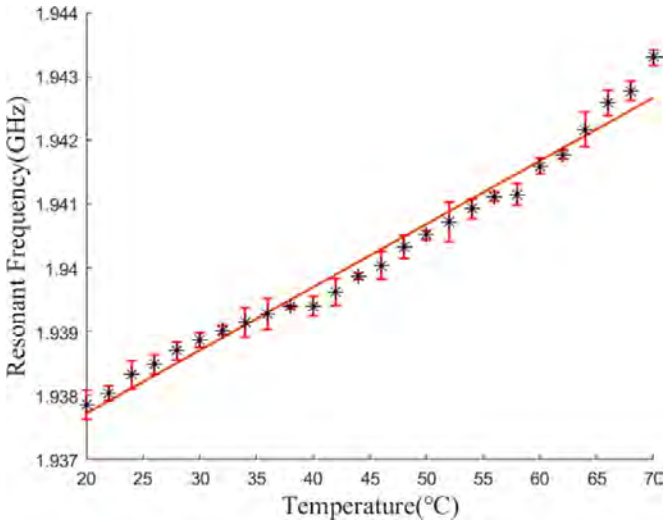

Figure 23. The resonant frequency in transverse direction under different temperatures.

sensitivity of 0.095 MHz $°C^{-1}$ in the transverse direction and 0.132 MHz $°C^{-1}$ in the longitudinal direction. The two fundamental resonant frequencies of the off-center fed patch antenna shift under different temperatures were approximately linear, and the linear trend of the resonant frequency is repeatable. The standard deviation of the resonant frequency under different temperatures was less than 0.152 MHz in transverse direction and 0.193 MHz in longitudinal direction. Thus, the patch antenna fundamental resonant frequency shift in the transverse direction can be measured by the VNA and the temperature sensing can be realized. The shift of the antenna's resonant frequency in the longitudinal direction can then be calculated at various temperatures.

To verify the patch antenna sensor performance under the condition that temperature and crack width change simultaneously, experimental tests were conducted with temperature changes from 20 °C to 60 °C with an increment of 5 °C, and the crack width changes from 0 mm to 0.6 mm with an increment of 0.2 mm. Figure 25 shows the patch antenna's resonant frequency in the longitudinal direction under different temperatures and different crack widths. The experimental results show that there exhibits a linear correlation between the resonant frequency in the longitudinal direction and the temperature. The variation of crack width also results in a quantitative change of resonant frequency in the longitudinal direction. Therefore, the off-center fed patch antenna sensor can measure the crack width and the temperature simultaneously.

Some differences occurred between the experimental results and the simulation results since the sensitivity of the patch antenna sensor for crack sensing is about 73% of the simulation results and the sensitivity for temperature sensing is about 71% of the simulation results. The main reason for the differences is that the environmental electromagnetic interference and the antenna fabrication both affected the sensitivity in experimental tests; therefore, the off-center fed patch antenna sensor is suggested to be calibrated to ensure measurement accuracy in practice.

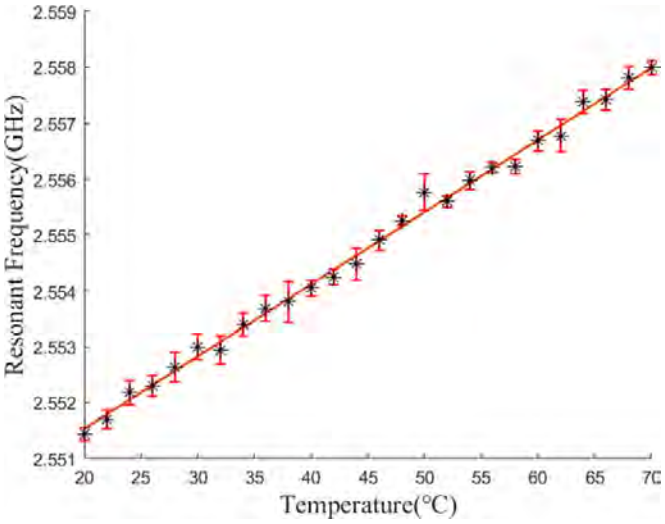

Figure 24. The resonant frequency in longitudinal direction under different temperatures.

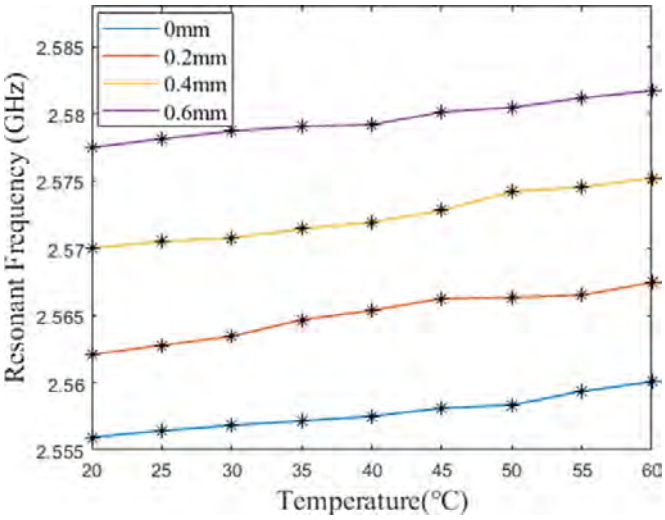

Figure 25. The resonant frequency with different crack widths under different temperatures.

5. Conclusions

This paper introduced a novel off-center fed patch antenna with overlapping sub-patch for simultaneous crack and temperature sensing. The off-center fed patch antenna with overlapping sub-patch is dual-resonant; thus, the crack width and temperature can be determined simultaneously from the patch antenna's resonant frequencies shifts. Moreover, the temperature sensing makes the patch antenna sensor suitable for temperature compensation. Theoretical study and simulations were conducted to study the shifts of patch antenna resonant frequencies with different crack widths and under different temperatures. In addition, a series of experimental tests were also conducted to demonstrate the feasibility and effectiveness of the proposed off-center fed patch antenna sensor for simultaneous crack and temperature sensing. Despite the encouraging results provided in this study, some significant concerns and problematic issues still need to be addressed, including the wireless interrogation technique and the investigation of higher temperature-sensitive dielectric substrate material, which will be investigated in future work.

Data availability statement

All data that support the findings of this study are included within the article (and any supplementary files).

Conflict of interest

The author(s) declare no potential conflicts of interest with respect to the research, authorship, and/or publication of this article.

Funding

This project is supported by the National Natural Science Foundation of China (Grant Nos. 52078375 and 52178298).

ORCID iDs

Xianzhi Li https://orcid.org/0000-0002-1314-5781
Liyu Xie https://orcid.org/0000-0001-5777-0645
Guochun Wan https://orcid.org/0000-0003-0521-1176

References

[1] Taheri S 2019 A review on five key sensors for monitoring of concrete structures *Constr. Build. Mater.* **204** 492–509
[2] Ou J P and Li H 2010 Structural health monitoring in mainland China: review and future trends *Struct. Health Monit.* **9** 219–31
[3] Yao Y, Tung S-T E and Glisic B 2014 Crack detection and characterization techniques—an overview *Struct. Control Health Monit.* **21** 1387–413
[4] Gong Q, Zhu L, Wang Y and Yu Z 2021 Automatic subway tunnel crack detection system based on line scan camera *Struct. Control Health Monit.* **28** e2776
[5] Li P, Qi Y, Yuan C, Kong Q and Xiong B 2021 A deep learning-based vision enhancement method for UAV assisted visual inspection of concrete cracks *Smart Struct. Syst.* **27** 1031–40
[6] Zhang Y and Yuen K-V 2021 Crack detection using fusion features-based broad learning system and image processing *Comput.-Aided Civ. Inf.* **36** 1568–84
[7] Kong S-Y, Fan J-S, Liu Y-F, Wei X-C and Ma X-W 2021 Automated crack assessment and quantitative growth monitoring *Comput.-Aided Civ. Inf.* **36** 656–74
[8] Wang B X, Zhao W G, Gao P, Zhang Y F and Wang Z 2018 Crack damage detection method via multiple visual features and efficient multi-task learning model *Sensors* **18** 1796
[9] Jahanshahi M R and Masri S F 2013 A new methodology for non-contact accurate crack width measurement through photogrammetry for automated structural safety evaluation *Smart Mater. Struct.* **22** 035019
[10] Dorafshan S, Thomas R J and Maguire M 2018 Comparison of deep convolutional neural networks and edge detectors for image-based crack detection in concrete *Constr. Build. Mater.* **186** 1031–45

[11] Gu X L, Chen Z Y and Ansari F 2000 Embedded fiber optic crack sensor for reinforced concrete structures *ACI Struct. J.* **97** 468–76

[12] Han T R, Wu G and Lu Y 2021 Crack monitoring using short-gauged Brillouin fiber optic sensor *Measurement* **179** 109461

[13] Sumant P S and Maiti S K 2006 Crack detection in a beam using PZT sensors *Smart Mater. Struct.* **15** 695–703

[14] Kocherla A, Duddi M and Subramaniam K V L 2021 Embedded PZT sensors for monitoring formation and crack opening in concrete structures *Measurement* **182** 109698

[15] Wang T, Tan B H, Lu M G, Zhang Z and Lu G 2020 Piezoelectric electro-mechanical impedance (EMI) based structural crack monitoring *Appl. Sci.* **10** 4648

[16] Qi C, Weixi Y, Jun L, Heming G and Yao M 2021 A research on fatigue crack growth monitoring based on multi-sensor and data fusion *Struct. Health Monit.* **20** 848–60

[17] Luo D, Yue Y C, Li P, Ma J X, Zhang L L, Ibrahim Z and Ismail Z 2016 Concrete beam crack detection using tapered polymer optical fiber sensors *Measurement* **88** 96–103

[18] Xu X and Huang H 2012 Battery-less wireless interrogation of microstrip patch antenna for strain sensing *Smart Mater. Struct.* **21** 125007

[19] Wan G, Kang W, Wang C, Li W, Li M, Xie L and Chen L 2021 Separating strain sensor based on dual-resonant circular patch antenna with chipless RFID tag *Smart Mater. Struct.* **30** 015007

[20] Zhang J, Tian G Y, Marindra A M, Sunny A I and Zhao A 2017 A review of passive RFID tag antenna-based sensors and systems for structural health monitoring applications *Sensors* **17** 265

[21] Yi X, Cho C, Cooper J, Wang Y, Tentzeris M M and Leon R T 2013 Passive wireless antenna sensor for strain and crack sensing—electromagnetic modeling, simulation, and testing *Smart Mater. Struct.* **22** 085009

[22] Xue S, Zheng Z, Guan S, Xie L, Wan G and Wan C 2020 A capacitively-fed inverted-F antenna for displacement detection in structural health monitoring *Sensors* **20** 5310

[23] Xue S, Yi Z, Xie L and Wan G 2021 Double-frequency passive deformation sensor based on two-layer patch antenna *Smart Struct. Syst.* **27** 969–82

[24] Xue S, Jiang K, Guan S, Xie L, Wan G and Wan C 2020 Long-range displacement meters based on chipped circular patch antenna *Sensors* **20** 4884

[25] Sanders J W, Yao J and Huang H Y 2015 Microstrip patch antenna temperature sensor *IEEE Sens. J.* **15** 5312–9

[26] Zhou S, Deng F, Yu L, Li B, Wu X and Yin B 2016 A novel passive wireless sensor for concrete humidity monitoring *Sensors* **16** 1535

[27] Xue S *et al* 2021 A bolt loosening detection method based on patch antenna with overlapping sub-patch *Struct. Health Monit.* 14759217211055613

[28] Yi Z, Xue S, Xie L and Wan G 2021 Detection of setting time in cement hydration using patch antenna sensor *Struct. Control Health Monit.* **29** e2855

[29] Cho C, Yi X, Li D, Wang Y and Tentzeris M M 2016 Passive wireless frequency doubling antenna sensor for strain and crack sensing *IEEE Sens. J.* **16** 5725–33

[30] Huang H, Farahanipad F and Singh A K 2017 A stacked dual-frequency microstrip patch antenna for simultaneous shear and pressure displacement sensing *IEEE Sens. J.* **17** 8314–23

[31] Chung K L, Wang L, Luo J, Li Y and Li Y 2020 Comparative study on directional sensitivity of patch-antenna-based strain sensors *Int. J. RF Microw. Comput.-Aided Eng.* **30** e22398

[32] Li D and Wang Y 2020 Thermally stable wireless patch antenna sensor for strain and crack sensing *Sensors* **20** 3835

[33] Sunny A I, Zhang J, Tian G Y, Tang C Q, Rafique W, Zhao A and Fan M 2019 Temperature independent defect monitoring using passive wireless RFID sensing system *IEEE Sens. J.* **19** 1525–32

[34] Fadamiro A O, Famoriji O J, Zakariyya R S, Lin F, Somefun O A, Ogunti E O, Apena W O and Dahunsi F M 2019 Temperature variation effect on a rectangular microstrip patch antenna *Int. J. Online Biomed. Eng.* **15** 101–18

[35] Maurya S 2013 Effect of temperature variation on microstrip patch antenna and temperature compensation technique *Int. J. Wirel. Commun. Mobil. Comput.* **1** 35–40

[36] Djerafi T, Wu K and Deslandes D 2012 A temperature-compensation technique for substrate integrated waveguide cavities and filters *IEEE Trans. Microw. Theory Tech.* **60** 2448–55

[37] Tchafa F M and Huang H 2018 Microstrip patch antenna for simultaneous strain and temperature sensing *Smart Mater. Struct.* **27** 065019

[38] Tchafa F M and Huang H 2019 Microstrip patch antenna for simultaneous temperature sensing and superstrate characterization *Smart Mater. Struct.* **28** 105009

[39] Caizzone S and DiGiampaolo E 2015 Wireless passive RFID crack width sensor for structural health monitoring *IEEE Sens. J.* **15** 6767–74

[40] Xue S, Xu K, Xie L and Wan G 2019 Crack sensor based on patch antenna fed by capacitive microstrip lines *Smart Mater. Struct.* **28** 085012

[41] Xue S, Yi Z, Xie L, Wan G and Ding T 2019 A passive wireless crack sensor based on patch antenna with overlapping sub-patch *Sensors* **19** 4327

[42] Ke L, Liu Z and Yu H 2019 Characterization of a patch antenna sensor's resonant frequency response in identifying the notch-shaped cracks on metal structure *Sensors* **19** 110

[43] Tung S-T and Glisic B 2016 Sensing sheet: the response of full-bridge strain sensors to thermal variations for detecting and characterizing cracks *Meas. Sci. Technol.* **27** 124010